
An Ideal Observer Model to Probe Human Visual Segmentation of Natural Images

Jonathan Vacher*

Albert Einstein College of Medicine
Dept. of Systems and Computational Biology
10461 Bronx, NY, USA
jonathan.vacher@einstein.yu.edu

Pascal Mamassian

Laboratoire des Systèmes Perceptifs, Département d'Études Cognitives
École Normale Supérieure, PSL Research University, CNRS
29 rue d'Ulm, 75005 Paris, France
pascal.mamassian@ens.fr

Ruben Coen-Cagli

Albert Einstein College of Medicine
Dept. of Systems and Computational Biology, and
Dominick P. Purpura Dept. of Neuroscience
10461 Bronx, NY, USA
ruben.coen-cagli@einstein.yu.edu

Abstract

Visual segmentation is a key perceptual function that partitions visual space and allows for detection, recognition and discrimination of objects in complex environments. The processes underlying human segmentation of natural images are still poorly understood. Existing datasets rely on manual labeling that conflate perceptual, motor, and cognitive factors. In part, this is because we lack an ideal observer model of segmentation to guide constrained experiments. On the other hand, despite recent progress in machine learning, modern algorithms still fall short of human segmentation performance. Our goal here is two-fold (i) propose a model to probe human visual segmentation mechanisms and (ii) develop an efficient algorithm for image segmentation. To this aim, we propose a novel probabilistic generative model of visual segmentation that for the first time combines 1) knowledge about the sensitivity of neurons in the visual cortex to statistical regularities in natural images; and 2) non-parametric Bayesian priors over segmentation maps (*ie.* partitions of the visual space). We provide an algorithm for learning and inference, validate it on synthetic data, and illustrate how the two components of our model improve segmentation of natural images. We then show that the posterior distribution over segmentations captures well the variability across human subjects, indicating that our model provides a viable approach to probe human visual segmentation.

1 Introduction

Visual segmentation is a core mechanism of biological vision, key to adaptive behavior in complex environments. For instance, it allows animals to detect upcoming danger, recognize their own kind,

*<https://jonathanvacher.github.io>
Preprint. Work in progress.

and discriminate between different types of food. Much effort has been devoted to develop image segmentation algorithms for artificial intelligence to improve environment-machine interactions (*eg.* autonomous cars, exploring robots, UAVs) and computer-aided diagnosis (*eg.* medical imaging and video surveillance), but existing algorithms often fall short of human performance. Our hypothesis is that efficient segmentation in humans and other primates relies on the sensitivity of visual cortical neurons to the statistics of natural images.

Segmentation in primate vision The segmentation of an image into individual objects and the integration of elementary features to build these objects are two competing and challenging tasks that the human visual system has to solve simultaneously. Much work in human visual psychophysics has focused on visual grouping and segmentation in simple artificial displays, such as boundaries between oriented textures, aligned edges forming a long contour embedded in randomly oriented distractors, simple shapes grouped by common motion patterns, and illusory edges and figures revealing perceptual expectations of simplicity and good continuation [45]. This work is mirrored by electrophysiology in non-human primates, which has revealed that neurons in early and mid-level areas of the visual cortex are sensitive to those segmentation cues [33, 38, 7, 21, 29]. As such, visual segmentation can be viewed as a feedforward process that is strongly refined and modulated by feedback and lateral connections [22] also allowing for fast peripheral detection of specific objects [6]. However, much less is known about segmentation of complex, natural images. Two notable exceptions are studies of contour grouping [17, 36] and figure-ground judgments [15], that showed how these processes rely largely on low-level image cues, thus suggesting a direct link between natural image statistics and segmentation.

Natural image statistics and cortical representations Natural images are characterized by the power-law decay of their power spectrum, and an abundance of oriented edges due, *eg.*, to occlusions and texture boundaries [43, 20]. Indeed, several unsupervised algorithms trained on natural images recover localized, oriented filters that are comparable with receptive fields (RFs) of neurons in primary visual cortex (V1) [27, 5], suggesting that V1 neurons represent over-complete wavelet coefficients of natural images. Importantly, images have also higher-order statistical structure, such as the nonlinear dependence between pairs of wavelet coefficients: the variance of one coefficient depends on the magnitude of the other coefficient [46]. These dependencies are captured well by Gaussian Scale Mixture (GSM) models, which assume that a latent global random variable (representing, *eg.*, contrast) scales a set of local Gaussian variables (representing the intensity of edges) thus introducing statistical coordination between wavelet coefficients [46]. GSM models have been used in practical applications, such as denoising [30, 32], contrast enhancement [23] and texture synthesis [42]. Furthermore, V1 neurons are sensitive to the dependencies described by the GSM [34], and probabilistic inference in mixtures of GSMs (mGSM; details in Section 2) explains nonlinear properties of V1 (*eg.* contextual modulation [11, 10] and temporal adaptation [39]) and achieves state-of-the-art predictions of V1 responses to natural images [12]. We will build on, and substantially extend, this class of models. Intuitively, the dependencies represented within the GSM reflect the properties that are shared within an object and that differ from other objects, thereby offering a natural strategy to segment the image.

Segmentation in computer vision Image segmentation in computer vision is a long standing topic, for review see *eg.* [28, 25, 13]. Because of the difficulty to gather large sets of human-segmented images, segmentation remains largely an unsupervised problem. For this reason, deep neural networks have had limited success, with the exception of the simpler problem of semantic segmentation [3, 9, 8]. The recent work of Xia *et al.* [47] tackles unsupervised segmentation, however the over-segmented output of their network requires substantial post-processing involving conditional Markov random field and hierarchical segmentation. Popular approaches to segmentation use graph-based methods [35, 14] which view an image as a graph to be partitioned. Approaches based on feature similarity are also common because they follow the idea that the human visual system tends to group together features that share the same properties [1, 26, 31]. Feature similarity can often be viewed as a statistical similarity, thus allowing for a probabilistic formulation. In addition, it is often combined with multi-scale approaches [1] and edge-based methods [2]. One of the most promising approaches is based on Bayesian probabilistic models. This is because they allow naturally to i) account for uncertainty in the assignment of an image patch to one of several possible segments (a prominent feature of human segmentation), and ii) incorporate knowledge about human segmentation strategies in the form of a Bayesian prior. Successful examples include probabilistic

mixture models with extensions of the natural Dirichlet Process (DP) prior, such as the distance dependent Chinese Restaurant Process [18], the spatially dependent Pitman-Yor process [40], and the Location Dependent Dirichlet Process (LDDP) [41], to restrain the search to partitions composed of contiguous component. This work however uses ad-hoc image descriptors and over-simplified assumptions about their statistics.

Contributions We will combine the strength of the Bayesian approach to segmentation, with accurate statistical models of the image features to which visual cortex is sensitive. We will focus on V1 because it has been studied extensively and it is strongly modulated by segmentation cues [38], but our approach could be easily extended hierarchically to include higher-level features, such as texture descriptors that capture V2 selectivity [16] and deep network layers that capture V4 and IT selectivity [48]. The statistics of V1-like image features (localized oriented filters) are accurately described by mGSMs, and V1 neurons are sensitive to the statistical similarity between features inside the RF and those in the surround in natural images [12]. Building on those results, here we propose a model in which multiple populations of model neurons perform statistical grouping of different regions of the visual field. Specifically, we associate each pixel to a feature vector consisting of neighboring wavelet coefficients (positions, orientations, scales) which are modeled by a mixture of GSMs (mGSM), and we adopt the hierarchical LDDP prior to encourage grouping of neurons sensitive to nearby areas of the visual field. We derive an efficient algorithm for learning and inference, validate it on synthetic data and natural images, and show that it captures uncertainty in human segmentations. Code is available online: <https://anonymized-address>.

Notations We will make use of the following notations. Integers D , N and K denote respectively the dimension, the number of samples and the number of classes/labels. A random variable is denoted by a capital letter X . The probability density function of X is denoted \mathbb{P}_X while x_i denotes a sample. The set Δ^K represents the K -dimensional simplex. Finally, “iid” stands for “independent identically distributed” while “pdf” stands for “probability density function”. Unless stated differently, all random variable are considered on the vector space \mathbb{R}^D provided with the Borel σ -algebra.

2 Towards an ideal observer model for visual segmentation

In this section, we introduce the different components of our model of visual segmentation. First, we briefly recall the GSM model for the local statistics of wavelet coefficients. Second, we describe the mGSM, which extends the GSM to account for the fact that natural images are not stationary signals. Lastly, we explain the LDDP prior. The full model is then discussed in the following section.

2.1 Gaussian scale mixture

Here we provide the general definition of GSM and describe the specific GSM we consider. Extensive descriptions of GSM models can be found elsewhere [46].

Definition 1 (GSM). *A random vector X is a Gaussian Scale Mixture if there exists a real random variable Z , a Gaussian random vector $G \sim \mathcal{N}(0, \Sigma)$, a bijective function $f \in \mathcal{C}^1(\mathbb{R}, \mathbb{R}_+)$ and $\mu \in \mathbb{R}$ such that $X = f(Z)G + \mu$.*

Remark 1. In the definition of GSM, the function f is generally omitted as it is often possible to directly compute the pdf of $\tilde{Z} = f(Z)$ from the pdf \mathbb{P}_Z of Z by variable substitution. In this case $X = \tilde{Z}G$ and the pdf of \tilde{Z} is $\mathbb{P}_{\tilde{Z}}(z) = \mathbb{P}_Z(f^{-1}(z)) \left| \frac{df^{-1}}{dz}(z) \right|$.

We consider the special case with $f(z) = \sqrt{z}$, and use for Z an Inverse-Gamma distribution $\gamma^{-1}(\alpha, \beta)$ with $\alpha, \beta > 0$, because in this case there is a closed form expression for the distribution of X , as follows:

Proposition 1. *If $X = \sqrt{Z}G + \mu$ with $\mu \in \mathbb{R}$, $Z \sim \gamma^{-1}(\alpha, \beta)$ and $G \sim \mathcal{N}(0, \Sigma)$ then X has the following pdf*

$$\mathbb{P}_X(x; \alpha, \beta, \mu, \Sigma) = \frac{\Gamma(D/2 + \beta) \alpha^{D/2}}{\Gamma(\beta) (2\pi)^{D/2} |\Sigma|^{1/2} (1 + \alpha/2(x - \mu)^T \Sigma^{-1} (x - \mu))^{D/2 + \beta}} \quad (1)$$

where $\Gamma(\beta) = \int_{\mathbb{R}_+} x^{\beta-1} e^{-x} dx$ is the Gamma function.

Remark 2. In the particular case where $\alpha = \frac{1}{\beta} = \frac{2}{\nu}$ where $\nu > 0$, \mathbb{P}_X is a multivariate extension of the Student-t distribution. In the following, we use $\alpha = 1$ because this scaling can be encoded in the covariance matrix Σ .

2.2 Mixture of Gaussian scale mixture

While the GSM captures well the local statistics of wavelet coefficients, it is well known that natural images are non-stationary signals. To illustrate this point, we took from the BSD dataset [24] an image with segments labeled by a human subject, and extracted different patches within each segment. Figure 1 shows that patches belonging to the same segment have less variable estimates of the GSM's mixing parameters β than patches from different segments. The non-stationary character of natural images is well captured by mixtures of GSMs (mGSM; see *eg.* [19]), defined as follows.

Definition 2 (mGSM). A random vector X is a K -mixture of Gaussian Scale Mixture where $K \in \mathbb{N}^*$ if there exist $(p_1, \dots, p_K) \in \Delta^K$ and K -GSM $(X^{(1)}, \dots, X^{(K)})$ such that, with probability p_k , $X \stackrel{d}{=} X^{(k)}$ where $\stackrel{d}{=}$ denotes equality in distribution.

The pdf of the random vector X is $\mathbb{P}_X = \sum_{k=1}^K p_k \mathbb{P}_{X^{(k)}}$.

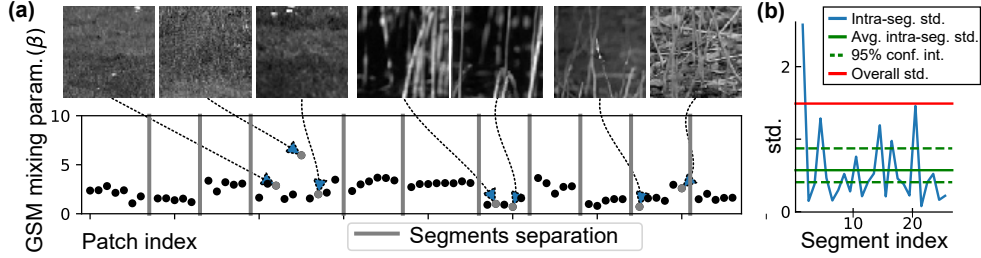


Figure 1: (a) Estimation of the mixing distribution parameter of the GSM (β) for some example natural image patches. Vertical gray lines separate patches belonging to the same segment identified by a human subject. (b) The estimated mixing parameters (β) of non-overlapping patches belonging to one segment show less variability (blue, average in green, confidence interval in green dotted line) than the overall variability (red) indicating that a mixture of GSM is a better model of natural image composed of multiple segments.

2.3 The Location Dependent Dirichlet Process

The Location Dependent Dirichlet Process (LDDP) introduced in [41] consists of the combination of a Dirichlet Process (DP) and an exponentiated Gaussian Process (GP). Such combination will allow to automatically select the number of components of the mixture, with a preference for components composed of contiguous sample points. The LDDP model assumes a notion of location for the data *ie.* each sample point x_n is associated to a physical location $l_n \in \mathbb{L}$ where \mathbb{L} is the lattice on which the data are observed. For instance, samples of sound amplitude are associated to a specific time while pixels of an image are associated to a spatial position. The following definition formalizes the LDDP.

Definition 3 (LDDP). The random function

$$P : \begin{cases} \mathbb{L} & \longrightarrow \Delta^K \\ l & \longmapsto (P_1(l), \dots, P_K(l)) \end{cases}$$

is a LDDP if there exists K independent Gamma random variables (Q_1, \dots, Q_K) and K independent Gaussian processes (F_1, \dots, F_K) with zero mean and, respectively, kernel functions (G_1, \dots, G_K) such that,

$$\forall k \in \{1, \dots, K\}, \quad \forall l \in L, \quad P_k(l) = \frac{Q_k e^{F_k(l)}}{\sum_{i=1}^K Q_i e^{F_i(l)}}.$$

In the following, we will consider iid Gamma random variables and iid stationary Gaussian processes so that the pdf are written

$$\mathbb{P}_Q(q; \lambda) = \frac{q^{\lambda-1} e^{-q}}{\Gamma(\lambda)} \quad \text{and} \quad \mathbb{P}_F(f; a, \sigma) = \frac{1}{(2\pi)^{N/2} |\bar{G}(a, \sigma)|^{1/2}} \exp\left(-\frac{1}{2} f^T \bar{G}(a, \sigma)^{-1} f\right)$$

where $\lambda > 0$ and $\bar{G}(a, \sigma)$ is a matrix derived from the stationary kernel function G with coefficients given by

$$\forall (m, n) \in \{1, \dots, N\}^2, \quad \bar{G}(a, \sigma)_{m,n} = G_{a,\sigma}(l_m - l_n) = a^2 \exp\left(-\frac{\|l_m - l_n\|^2}{2\sigma^2}\right)$$

with $a, \sigma > 0$.

3 Segmentation inference by expectation-maximization

The full model we consider is a mGSM (Section 2.2) with a LDDP prior (Section 2.3) on the mixing probabilities of the mixture. To train our model, we adopt the Expectation-Maximization (EM) approach which consists in completing the sample data with their class. Therefore, we consider $((x_n, c_n))_{n \in \{1, \dots, N\}}$ where for all n , $c_n \in \{1, \dots, K\}$ is the class of x_n and we use the maximum a posteriori (MAP) estimator

$$\begin{aligned} \hat{\theta} &= \underset{\theta}{\operatorname{argmax}} \mathbb{P}_{\Theta|(X_n, C_n)_n}(\theta; (x_n, c_n)_n) = \underset{\theta}{\operatorname{argmax}} \mathbb{P}_{(X_n, C_n)_n|\Theta}((x_n, c_n)_n; \theta) \mathbb{P}_{\Theta}(\theta) \\ &= \underset{\theta}{\operatorname{argmax}} \mathbb{P}_{\Theta}(\theta) \prod_{n=1}^N \mathbb{P}_{X_n, C_n|\Theta}(x_n, c_n; \theta) \\ &= \underset{\theta}{\operatorname{argmax}} \mathbb{P}_{\Theta}(\theta) \prod_{n=1}^N \prod_{k=1}^K \left(\frac{q_k e^{f_k(l_n)}}{\sum_i q_i e^{f_i(l_n)}} \mathbb{P}_{X^{(k)}}(x_n; \beta_k, \mu_k, \Sigma_k) \right)^{\mathbb{1}_k(c_n)} \\ &= \underset{\theta}{\operatorname{argmin}} l((x_n, c_n)_n; \theta) \end{aligned}$$

with $\theta = (\mathbf{q}, \mathbf{f}, \boldsymbol{\beta}, \boldsymbol{\mu}, \boldsymbol{\Sigma}) = ((q_k)_k, (f_k)_k, (\beta_k)_k, (\mu_k)_k, (\Sigma_k)_k)$ and $\mathbb{1}_k(c) = 1$ if $c = k$ and $\mathbb{1}_k(c) = 0$ otherwise, and where l is the negative log-posterior function

$$\begin{aligned} l((x_n, c_n)_n; \theta) &= - \sum_{n=1}^N \sum_{k=1}^K \mathbb{1}_k(c_n) \log \left(\frac{q_k e^{f_k(l_n)}}{\sum_i q_i e^{f_i(l_n)}} \mathbb{P}_{X^{(k)}}(x_n; \beta_k, \mu_k, \Sigma_k) \right) \\ &\quad - \sum_{k=1}^K [\log(\mathbb{P}_Q(q_k; \lambda)) + \log(\mathbb{P}_F(f_k; a, \sigma))], \end{aligned}$$

Note that we use a proper prior for the variables (\mathbf{q}, \mathbf{f}) while we use an improper constant prior for the variables $(\boldsymbol{\beta}, \boldsymbol{\mu}, \boldsymbol{\Sigma})$. This contrasts with the original LDDP [41] where they use a Gaussian-Wishart distribution for $(\boldsymbol{\mu}, \boldsymbol{\Sigma})$. However, our choice simplifies the maximization step in the EM algorithm.

The expectation step is standard for mixture distributions and only requires the computation of the posterior assignment of pixels to segments, at the t -th iteration

$$\tau_{n,k}^{(t)} \stackrel{\text{def}}{=} \mathbb{E}(\mathbb{1}_k(C_n) | x_n, \boldsymbol{\theta}^{(t)}) = \mathbb{P}_{C_n | X_n, \Theta}(k | x_n, \boldsymbol{\theta}^{(t)}) = \frac{p_k^{(t)}(l_n) \mathbb{P}_{X^{(k)}}(x_n; \beta_k^{(t)}, \mu_k^{(t)}, \Sigma_k^{(t)})}{\sum_{i=1}^K p_i^{(t)}(l_n) \mathbb{P}_{X^{(i)}}(x_n; \beta_i^{(t)}, \mu_i^{(t)}, \Sigma_i^{(t)})}$$

$$\text{with } p_k^{(t)}(l_n) = \frac{q_k^{(t)} e^{f_k^{(t)}(l_n)}}{\sum_i q_i^{(t)} e^{f_i^{(t)}(l_n)}}.$$

Then, the maximization step involves minimizing the expectation of the completed-data negative log-posterior

$$\begin{aligned} Q(\boldsymbol{\theta}; \boldsymbol{\theta}^{(t)}, (x_n)_n) &= - \sum_{n=1}^N \sum_{k=1}^K \tau_{n,k}^{(t)} \left[\log(q_k) + f_k(l_n) - \log \left(\sum_i q_i e^{f_i(l_n)} \right) + \log \left(\Gamma \left(\beta + \frac{D}{2} \right) \right) \right. \\ &\quad \left. - \log(\Gamma(\beta_k)) - \frac{1}{2} \log(|\Sigma_k|) - \left(\frac{D}{2} + \beta_k \right) \log \left(1 + \frac{1}{2} d_{\Sigma_k}(x_n, \mu_k)^2 \right) \right] \\ &\quad - \sum_{k=1}^K [(\lambda - 1) \log(q_k) - q_k - \frac{1}{2} f_k^T \bar{G}(a, \sigma)^{-1} f_k] \end{aligned}$$

where $d_{\Sigma}(x, \mu) = \sqrt{(x - \mu)^T \Sigma^{-1} (x - \mu)}$ is the Mahalanobis distance.

Proposition 2. *At an extremum point of Q , the following equations hold for all $k \in \{1, \dots, K\}$*

$$\mu_k = \frac{\sum_{n=1}^N \tau_{n,k}^{(t)} \omega(x_n, \beta_k, \mu_k, \Sigma_k) x_n}{\sum_{n=1}^N \tau_{n,k}^{(t)} \omega(x_n, \beta_k, \mu_k, \Sigma_k)}, \quad (2)$$

$$\Sigma_k = \frac{\sum_{n=1}^N \tau_{n,k}^{(t)} \omega(x_n, \beta_k, \mu_k, \Sigma_k) (x_n - \mu_k)(x_n - \mu_k)^T}{\sum_{n=1}^N \tau_{n,k}^{(t)}}, \quad (3)$$

$$\psi(\beta_k) - \psi(D/2 + \beta_k) + \log \left(1 + \frac{1}{2} d_{\Sigma_k}(x, \mu_k)^2 \right) = 0, \quad (4)$$

$$q_k = \lambda - 1 + \sum_{n=1}^N \tau_{n,k}^{(t)} - p_k(l_n) \quad (5) \quad f_k = \bar{G}(a, \sigma)(\tau_{\cdot,k}^{(t)} - p_k(\cdot)) \quad (6)$$

where $\omega(x, \beta, \mu, \Sigma) = \frac{D+2\beta}{2+d_{\Sigma}(x, \mu)^2}$, $\psi(x) = \frac{\Gamma'(x)}{\Gamma(x)}$ is the digamma function and $p_k(l_n) = \frac{q_k e^{f_k(l_n)}}{\sum_i q_i e^{f_i(l_n)}}$.

The four equations of Proposition 2 have no closed form solutions. However, in such form, Equations (2), (3), (5) and (6) can be solved recursively by using their estimates from the last iteration of EM ($\mathbf{q}^{(t)}$, $\mathbf{f}^{(t)}$, $\beta^{(t)}$, $\mu^{(t)}$, $\Sigma^{(t)}$) in the right hand terms. Specifically, Equation (4) requires both the last estimates of the parameters and a numerical step to update β (Newton-Raphson). We noticed that Equation (5) recursively sometimes generates negative values, which are not admissible. We prevent this by projecting $\tau_{n,k}^{(t)} - p_k(l_n)$ onto \mathbb{R}^+ . Although numerical experiments show that the local convergence property of EM algorithm is lost (see Supplementary Figure 1), we found it is preserved for sufficiently small σ , as we illustrate next.

Numerical experiment on synthetic data We tested our algorithm numerically on synthetic datapoints generated from our model with $N = 10000$ samples and $K = 3$ classes. In the top row of Figure 2 we compared the behavior of the log-posterior and parameter estimates during the EM steps with the Student+DP algorithm. The Student+DP algorithm is a direct implementation of the classical EM algorithm, so it converges to a local minimum and the negative log-posterior is strictly decreasing. This is not true in general for our algorithm because of the projection required to avoid negative q_k , but with small σ (< 0.01) we find that the log-posterior is strictly decreasing. Note that this small value of σ is assumed when fitting the model, but data were generated with a larger values (> 100). Both algorithms achieve similar relative error for the parameters' estimates. Supplementary Figure 1 shows that with larger σ the negative log-posterior does not decrease monotonically, yet the parameter estimates reach the same level of relative error as for the Student+DP algorithm. Then, larger values of σ are acceptable when inferring segmentation of natural images. The bottom row of Figure 2 shows also that our algorithm correctly identifies the number of clusters, and that the assignment of individual datapoints to clusters is accurate for more than 99% of the cases (averaged over 10 test sets).

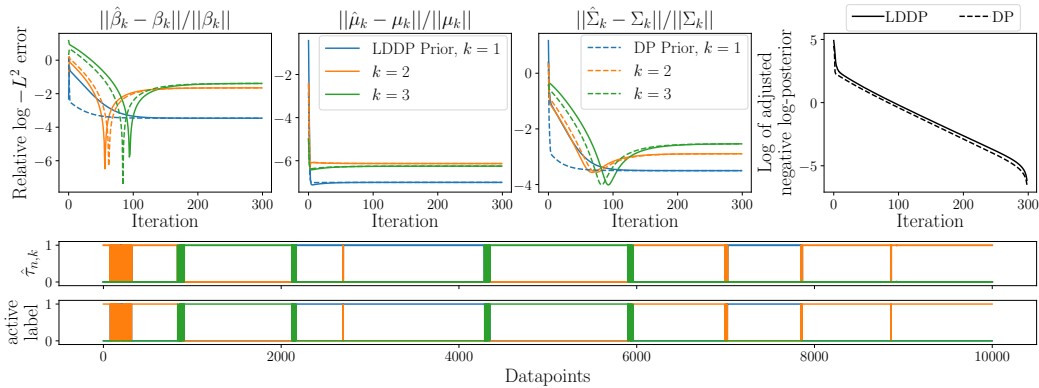


Figure 2: *Top row: relative error with the ground truth parameters as a function of iteration and the corresponding negative log-posterior. Bottom row, from top to bottom: estimated prior mixing probabilities, estimated posterior mixing probabilities and ground truth prior probabilities.*

4 Results

In this section we present segmentation results and compare our model, i.e. mGSM likelihood combined with LDDP, to (i) the model of [41], i.e. Gaussian likelihood combined with LDDP prior, and (ii) mGSM likelihood combined with DP prior. Such comparisons allow us to evaluate separately the advantage of the mGSM likelihood and the LDDP prior.

We tested the models on the BSD database of natural images with segmentations performed by human subjects [24, 2]. We first illustrate qualitative differences between the models, and quantify their match to human segmentations using a standard metric, the Rand index [44]. We then address uncertainty in segmentation, and compare the models on their ability to capture uncertainty in the human data.

Segmentation performance In our implementation, we associate to each pixel of the image a vector of V1-like features consisting of 4 orientations and 3 spatial frequencies (or scales) obtained from the steerable pyramid [37]. We reduce the dimension of the feature vectors from 12 to 8 using PCA (a sharp cutoff is visible in the eigenvalues of the covariance matrix). We set the parameters to: $\lambda = 0.07$, $K = 8$ and $a = 10$, $\sigma = 5$ when LDDP prior is used.

Figure 3 shows the original images, segmentations by two humans, and the segmentations obtained with the three algorithms (additional examples are shown in supplementary Section 2). For mGSM+DP the segmentation map is extremely noisy and the bears are not well separated from the background, reflecting the lack of a prior on spatial structure. Adding the LDDP prior to the mGSM reduces local noise substantially and improves the segmentation: we are able to clearly identify the foreground and background segments, and different bears are segmented separately. The segmentation obtained with Gaussian+LDDP algorithm is smoother than mGSM+DP, as expected thanks to the prior. However, it still contains noisy areas where segments are intermingled. Using the mGSM mitigates this issue because it can account separately for local variations in texture (the local variables in the GSM) as well as contrast (the GSM mixer). Quantitatively, the Rand index for our mGSM+LDDP is twice as high as the Gaussian+LDDP (0.29 for mGSM versus 0.16 for Gaussian), confirming the advantage of a likelihood model that captures natural image statistics accurately.

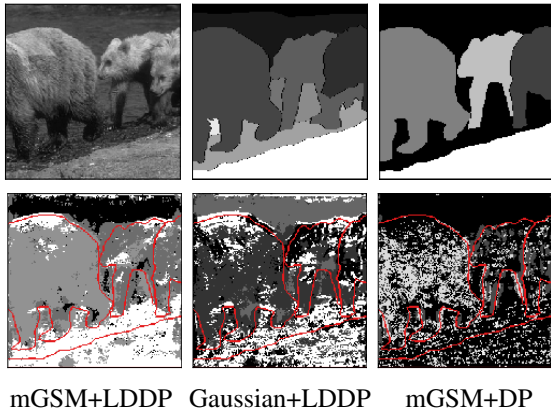


Figure 3: *Top row: original image and 2 corresponding human segmentation. Bottom row: results of segmentation obtained with 3 algorithms: mGSM+LDDP, Gaussian+LDDP and mGSM+DP. Red lines: human segmentation boundaries*

Segmentation uncertainty To fully capture human segmentation, we need to account also for the uncertainty that often accompanies perception due to ambiguity and noise in the sensory signals [4]. For instance, the segmentation of pixels near the boundary between similar textures (eg. around the legs in 3) is more uncertain than those inside the fur. This motivated our choice of probabilistic segmentation algorithms, as they naturally account for uncertainty by providing a probability distribution over partitions which we could compare to human uncertainty.

Unfortunately, no experimental data are currently available for segmentation uncertainty in individual subjects. However, we took advantage of the fact that BSD images are segmented by several subjects, and we used variability across subjects as a proxy for uncertainty. Specifically, we measured the probability, over the multiple human segmentation maps, that two pixels belong to the same segment: the closer this probability is to 0.5, the higher the uncertainty. Figure 4a shows an example of a reference pixel n_0 (indicated by the cross) and its corresponding mean map (the probability $p(c_n = c_{n_0})$ that other pixels belong to the same segment). Variability is generally high around edges, but it can also be high for large background areas that are segmented with more or less precision.

We summarize the map for the mean in Figure 4b by averaging the value of $p(c_n = c_{n_0})$ across all points n within an annulus at distance r and across multiple reference pixel n_0 . We thus obtain an estimate of the probability that two pixels belong to the same segment as a function of their distance r . As expected, we find that humans tend to group nearby pixels together, which motivated the use of the LDDP in the first place. Furthermore, for any fixed r , different reference points can have vastly different probability (i.e. the spread on the abscissa in Figure 4c), and hence different uncertainty. A good model of human segmentation should capture this uncertainty. We therefore compared humans and models across different reference points and distances in Figure 4c. We found that the Gaussian+LDDP had a good correlation, thanks to the localized prior, and that the use of the mGSM likelihood substantially improved the match between model and human uncertainty. Notice also (Figure 4b, and points in the bottom-right of Figure 4c) that the LDDP does not fully capture the tendency of humans to group together neighboring pixels, suggesting a direction for future improvement.

Together, these results indicate our approach represents a substantial step forward in achieving an ideal observer model to probe human visual segmentation.

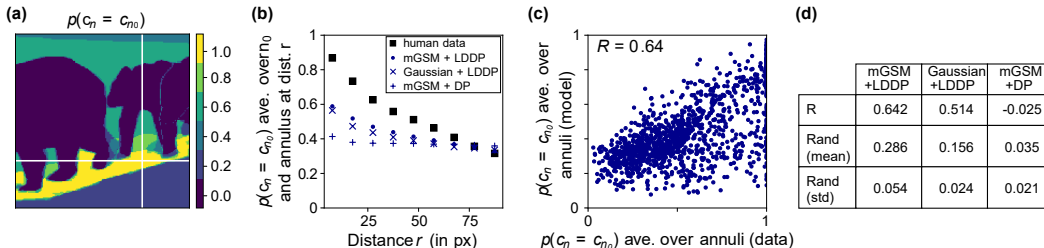


Figure 4: **(a)** Probability $p(c_n = c_{n_0})$ that other pixels belong to the same segment. **(b)** Probability that two pixels have belong to the same segment as a function of distance r . **(c)** Correlation between human data and model of the average of $p(c_n = c_{n_0})$ over different annuli at distance r . **(d)** Correlation of **(c)** for the three models and the Rand index average and standard deviation (the average corresponds to the probabilistic Rand index).

5 Conclusion and future work

We have proposed an ideal observer model of visual segmentation that combines the mGSM likelihood, which is a powerful model of the statistics of low-level features in natural images, with the LDDP prior to enforce a preference for contiguous partitions.

Training this kind of hierarchical models can be challenging; here we have provided an approximate inference algorithm based on EM, and demonstrated on synthetic data that it behaves well and recovers the ground truth parameters and segmentation labels with high accuracy. When tested on gray-scale images, our algorithm produces good segmentations and also captures human variability. These experiments also demonstrate that the LDDP prior and the mGSM likelihood confer complementary advantages, suggesting two clear directions for improvement. First, a natural extension will be to include higher-level visual features and extend the likelihood model to capture their statistical dependencies. Secondly, the algorithm could be refined by developing automatic parameter selection for the prior and adding *ad-hoc* innovation terms in the prior to better explore the space of partitions.

Together, our results indicate that combining knowledge about image statistics and neural coding in the visual cortex can improve probabilistic models of image segmentation, and pave the road towards controlled experiments on human visual segmentation.

References

- [1] S. Alpert, M. Galun, A. Brandt, and R. Basri. Image segmentation by probabilistic bottom-up aggregation and cue integration. *IEEE transactions on pattern analysis and machine intelligence*, 34(2):315–327, 2012.
- [2] P. Arbelaez, M. Maire, C. Fowlkes, and J. Malik. Contour detection and hierarchical image segmentation. *IEEE transactions on pattern analysis and machine intelligence*, 33(5):898–916, 2011.
- [3] V. Badrinarayanan, A. Kendall, and R. Cipolla. Segnet: a deep convolutional encoder-decoder architecture for image segmentation. *IEEE transactions on pattern analysis and machine intelligence*, 39(12):2481–2495, 2017.
- [4] S. Barthelmé and P. Mamassian. Evaluation of objective uncertainty in the visual system. *PLoS computational biology*, 5(9):e1000504, 2009.
- [5] A. J. Bell and T. J. Sejnowski. The “independent components” of natural scenes are edge filters. *Vision research*, 37(23):3327–3338, 1997.
- [6] M. Boucart, Q. Lenoble, J. Quettelart, S. Szaffarczyk, P. Desprez, and S. J. Thorpe. Finding faces, animals, and vehicles in far peripheral vision. *Journal of vision*, 16(2):10–10, 2016.
- [7] J. R. Cavanaugh, W. Bair, and J. A. Movshon. Nature and interaction of signals from the receptive field center and surround in macaque v1 neurons. *Journal of neurophysiology*, 88(5):2530–2546, 2002.
- [8] L.-C. Chen, G. Papandreou, I. Kokkinos, K. Murphy, and A. L. Yuille. Deeplab: semantic image segmentation with deep convolutional nets, atrous convolution, and fully connected crfs. *IEEE transactions on pattern analysis and machine intelligence*, 40(4):834–848, 2018.
- [9] L.-C. Chen, Y. Zhu, G. Papandreou, F. Schroff, and H. Adam. Encoder-decoder with atrous separable convolution for semantic image segmentation. *arXiv preprint arXiv:1802.02611*, 2018.
- [10] R. Coen-Cagli, P. Dayan, and O. Schwartz. Cortical surround interactions and perceptual salience via natural scene statistics. *PLoS Computational Biology*, 8(3), 2012.
- [11] R. Coen-Cagli, P. Dayan, and O. Schwartz. Statistical models of linear and nonlinear contextual interactions in early visual processing. In *Advances in neural information processing systems*, pages 369–377, 2009.
- [12] R. Coen-Cagli, A. Kohn, and O. Schwartz. Flexible gating of contextual influences in natural vision. *Nature Neuroscience*, 18(11):1648, 2015.
- [13] V. Dey, Y. Zhang, and M. Zhong. A review on image segmentation techniques with remote sensing perspective, 2010.
- [14] P. F. Felzenszwalb and D. P. Huttenlocher. Efficient graph-based image segmentation. *International journal of computer vision*, 59(2):167–181, 2004.
- [15] C. C. Fowlkes, D. R. Martin, and J. Malik. Local figure–ground cues are valid for natural images. *Journal of Vision*, 7(8):2–2, 2007.
- [16] J. Freeman, C. M. Ziemba, D. J. Heeger, E. P. Simoncelli, and J. A. Movshon. A functional and perceptual signature of the second visual area in primates. *Nature neuroscience*, 16(7):974, 2013.
- [17] W. S. Geisler and J. S. Perry. Contour statistics in natural images: grouping across occlusions. *Visual neuroscience*, 26(1):109–121, 2009.
- [18] S. Ghosh, A. B. Ungureanu, E. B. Sudderth, and D. M. Blei. Spatial distance dependent chinese restaurant processes for image segmentation. In *Advances in Neural Information Processing Systems*, pages 1476–1484, 2011.
- [19] J. A. Guerrero-Colón, E. P. Simoncelli, and J. Portilla. Image denoising using mixtures of gaussian scale mixtures. In *Image Processing, 2008. ICIP 2008. 15th IEEE International Conference on*, pages 565–568. IEEE, 2008.
- [20] A. Hyvärinen, J. Hurri, and P. O. Hoyer. *Natural image statistics: a probabilistic approach to early computational vision*. Springer.

- [21] W. Li, V. Piëch, and C. D. Gilbert. Contour saliency in primary visual cortex. *Neuron*, 50(6):951–962, 2006.
- [22] Z. Li. Contextual influences in v1 as a basis for pop out and asymmetry in visual search. *Proceedings of the National Academy of Sciences*, 96(18):10530–10535, 1999.
- [23] S. Lyu and E. P. Simoncelli. Nonlinear image representation using divisive normalization. In *Computer Vision and Pattern Recognition, 2008. CVPR 2008. IEEE Conference on*, pages 1–8. IEEE, 2008.
- [24] D. Martin, C. Fowlkes, D. Tal, and J. Malik. A database of human segmented natural images and its application to evaluating segmentation algorithms and measuring ecological statistics. In *Proc. 8th Int’l Conf. Computer Vision*, volume 2, pages 416–423, July 2001.
- [25] J.-M. Morel and S. Solimini. *Variational methods in image segmentation: with seven image processing experiments*, volume 14. Springer Science & Business Media, 2012.
- [26] J. Ning, L. Zhang, D. Zhang, and C. Wu. Interactive image segmentation by maximal similarity based region merging. *Pattern Recognition*, 43(2):445–456, 2010.
- [27] B. A. Olshausen and D. J. Field. Emergence of simple-cell receptive field properties by learning a sparse code for natural images. *Nature*, 381(6583):607, 1996.
- [28] N. R. Pal and S. K. Pal. A review on image segmentation techniques. *Pattern recognition*, 26(9):1277–1294, 1993.
- [29] A. Pasupathy. The neural basis of image segmentation in the primate brain. *Neuroscience*, 296:101–109, 2015.
- [30] J. Portilla, V. Strela, M. J. Wainwright, and E. P. Simoncelli. Image denoising using scale mixtures of gaussians in the wavelet domain. *IEEE Transactions on Image processing*, 12(11):1338–1351, 2003.
- [31] J. Puzicha, T. Hofmann, and J. M. Buhmann. Non-parametric similarity measures for unsupervised texture segmentation and image retrieval. In *Computer Vision and Pattern Recognition, 1997. Proceedings., 1997 IEEE Computer Society Conference on*, pages 267–272. IEEE, 1997.
- [32] Y. Rakvongthai, A. P. Vo, and S. Orintara. Complex gaussian scale mixtures of complex wavelet coefficients. *IEEE Transactions on Signal Processing*, 58(7):3545–3556, 2010.
- [33] P. R. Roelfsema. Cortical algorithms for perceptual grouping. *Annu. Rev. Neurosci.*, 29:203–227, 2006.
- [34] O. Schwartz and E. P. Simoncelli. Natural signal statistics and sensory gain control. *Nature neuroscience*, 4(8):819, 2001.
- [35] J. Shi and J. Malik. Normalized cuts and image segmentation. *IEEE Transactions on pattern analysis and machine intelligence*, 22(8):888–905, 2000.
- [36] M. Sigman, G. A. Cecchi, C. D. Gilbert, and M. O. Magnasco. On a common circle: natural scenes and gestalt rules. *Proceedings of the National Academy of Sciences*, 98(4):1935–1940, 2001.
- [37] E. P. Simoncelli and W. T. Freeman. The steerable pyramid: a flexible architecture for multi-scale derivative computation. In *Image Processing, 1995. Proceedings., International Conference on*, volume 3, pages 444–447. IEEE, 1995.
- [38] A. M. Sillito, K. L. Grieve, H. E. Jones, J. Cudeiro, and J. Davls. Visual cortical mechanisms detecting focal orientation discontinuities. *Nature*, 378(6556):492, 1995.
- [39] M. Snow, R. Coen-Cagli, and O. Schwartz. Specificity and timescales of cortical adaptation as inferences about natural movie statistics. *Journal of vision*, 16(13), 2016.
- [40] E. B. Sudderth and M. I. Jordan. Shared segmentation of natural scenes using dependent pitman-yor processes. In *Advances in neural information processing systems*, pages 1585–1592, 2009.
- [41] S. Sun, J. Paisley, and Q. Liu. Location dependent dirichlet processes. In *International Conference on Intelligent Science and Big Data Engineering*, pages 64–76. Springer, 2017.
- [42] L. Theis, R. Hosseini, and M. Bethge. Mixtures of conditional gaussian scale mixtures applied to multiscale image representations. *PLoS One*, 7(7):e39857, 2012.
- [43] A. Torralba and A. Oliva. Statistics of natural image categories. *Network: computation in neural systems*, 14(3):391–412, 2003.
- [44] R. Unnikrishnan, C. Pantofaru, and M. Hebert. Toward objective evaluation of image segmentation algorithms. *IEEE transactions on pattern analysis and machine intelligence*, 29(6):929–944, 2007.

- [45] J. Wagemans, J. H. Elder, M. Kubovy, S. E. Palmer, M. A. Peterson, M. Singh, and R. von der Heydt. A century of gestalt psychology in visual perception: i. perceptual grouping and figure-ground organization. *Psychological bulletin*, 138(6):1172, 2012.
- [46] M. J. Wainwright and E. P. Simoncelli. Scale mixtures of gaussians and the statistics of natural images. In *Advances in neural information processing systems*, pages 855–861, 2000.
- [47] X. Xia and B. Kulis. W-net: a deep model for fully unsupervised image segmentation. *arXiv preprint arXiv:1711.08506*, 2017.
- [48] D. L. Yamins, H. Hong, C. F. Cadieu, E. A. Solomon, D. Seibert, and J. J. DiCarlo. Performance-optimized hierarchical models predict neural responses in higher visual cortex. *Proceedings of the National Academy of Sciences*, 111(23):8619–8624, 2014.